

**Growth of  $^{18}\text{O}$  isotopically-enriched ZnO nanorods by two novel VPT methods**

Ciarán Gray<sup>1,\*</sup>, Lukas Trefflich<sup>2</sup>, Robert Röder<sup>2</sup>, Carsten Ronning<sup>2</sup>, Martin O. Henry<sup>1</sup>, Enda McGlynn<sup>1,\*</sup>

<sup>1</sup> *School of Physical Sciences, National Centre for Plasma Science and Technology, Dublin City University, Glasnevin, Dublin 9, Ireland.*

<sup>2</sup> *Institute of Solid State Physics, Friedrich-Schiller-University of Jena, 07743 Jena, Germany.*

ciaran.gray5@mail.dcu.ie

enda.mcglynn@dcu.ie

\*Correspondence should be addressed.

**ABSTRACT**

We have developed two novel vapour phase transport methods to grow ZnO nanorod arrays isotopically enriched with  $^{18}\text{O}$ . Firstly, a three-step process used to grow natural and Zn-enriched ZnO nanorods has been further modified, by replacing the atmospheric  $\text{O}_2$  with enriched  $^{18}\text{O}_2$ , in order to grow  $^{18}\text{O}$ -enriched ZnO nanorods using this vapour-solid method on chemical bath deposited buffer layers. In addition,  $^{18}\text{O}$ -enriched ZnO nanorods were successfully grown using isotopically  $^{18}\text{O}$ -enriched ZnO source powders in a vapour-liquid-solid growth method. Scanning electron microscopy studies confirmed the success of both growth methods in terms of nanorod morphology, although in the case of the vapour-liquid-solid samples, the nanorods'  $c$ -axes were not vertically aligned due to the use of a non-

epitaxial substrate. Raman and PL studies indicated clearly that O-enrichment was successful in both cases, although the results indicate that the enrichment is at a lower level in our samples compared to previous reports with the same nominal enrichment levels. The results of our studies also allow us to comment on both levels of enrichment achieved and on novel effects of the high temperature growth environment on the nanorod growth, as well as suggesting possible mechanisms for such effects. Very narrow photoluminescence line widths, far narrower than those reported previously in the literature for isotopically enriched bulk ZnO, are seen in both the vapour-solid and vapour-liquid-solid nanorod samples demonstrating their excellent optical quality and their potential for use in detailed optical studies of defects and impurities using low temperature photoluminescence.

KEYWORDS: A1. Characterization, A1. Nanostructures, A2. Growth from vapour, B1. Zinc compounds, B2. Semiconducting II-VI materials.

## 1. INTRODUCTION

ZnO nanostructures have been synthesized in a wide variety of different morphologies. These include thin films [1], nanorods, nanowires[2–5], nanowalls[6], nanodisks[7], and a range of other “nano” morphologies [8,9]. The production of ZnO nanorods for use in optical and nano-optoelectronic applications and studies is of particular interest [10–12]. Growth of ZnO nanostructures using high temperature methods such as vapour phase transport (VPT) leads to very high quality material demonstrating excellent single crystallinity and optical properties because the small nanostructure footprint reduces the generation of extended defects associated with lattice mismatch with the substrate. Furthermore, nanostructure growth also potentially enables relatively simple control of

isotopic concentrations since the amounts of source material as well as material being produced are relatively small. Isotopic enrichment is a very useful technique in the study of impurities in semiconductor materials such as ZnO, particularly using optical methods where shifts in spectral features can provide important information on the properties (including chemical constituents) of both intrinsic and defect-related optical features [13–18]. Reports using isotopically enriched bulk single crystal ZnO samples have included studies of bandgap energies, phonon frequencies and linewidths and heat capacity. However in all cases these samples had quite poor optical quality, e.g. reported photoluminescence (PL) linewidths of ~5 meV and ~2-8 meV [19,20].

The use of isotopically enriched nanostructured material allows us to combine the two key advantages mentioned above (excellent optical quality and control of isotopic concentration) for the study of the optical properties of the semiconductor material. Recently, we reported for the first time the successful growth of Zn-isotopically enriched ZnO nanorods by a VPT process on chemical bath deposition (CBD)-grown buffer layers, which showed good isotopic enrichment and excellent optical properties [21]. In the present work, we report two relatively fast, easy, reliable and novel methods of growing O-isotopically enriched ZnO nanorods of very high crystalline quality, which display excellent optical quality as determined by low temperature PL studies. The samples produced here are suitable for detailed defect studies. We have grown ZnO nanorod samples enriched with  $^{18}\text{O}$  and  $^{16/18}\text{O}$ , as well as natural  $^{16}\text{O}$  samples using these two novel growth methods.

Furthermore, our studies allow us to comment on both the levels of enrichment achieved and on some effects of the high temperature growth environment on the nanorod growth. Our data show that the source of  $^{16}\text{O}$  contamination must come from sources of oxygen already chemically bound within the growth system and we discuss three potential mechanisms

relevant to different samples; (i) diffusion/migration of  $^{16}\text{O}$  from the unenriched buffer layer in the case of the VS samples, (ii) exchange of  $^{18}\text{O}$  with  $^{16}\text{O}$  in the polycrystalline quartz/alumina tubes/boats at high temperature and (iii) the ubiquitous presence of adsorbed water layers on all surfaces in the growth system which could lead to an exchange of  $^{18}\text{O}$  with  $^{16}\text{O}$ , acting as a source of  $^{16}\text{O}$  contamination.

## 2. MATERIALS AND METHODS

### 2.1. Modified Vapour-Solid CTR-VPT method

This growth method is a three step process involving the deposition of an initial buffer layer of ZnO nanorods using drop coating and CBD, followed by the main growth of the nanorods using carbothermal reduction VPT (CTR-VPT). CBD, VPT and CTR-VPT are well established methods used to grow ZnO nanorods [2,5,22–24]. This specific growth method used here is described in the following references [2,3,25]. It was previously modified to produce Zn-enriched nanorods as reported recently [21] and is further modified here to produce  $^{18}\text{O}$ - isotope enriched nanorods.

The ZnO nanorods were grown on Si (100) substrates 0.5 mm thick and 1-4 cm<sup>2</sup> in area. The first stage of the growth process, seed layer preparation, was carried out as described in reference [21]. This process produces a thin layer (< 25 nm) [26] of crystallographically aligned ZnO crystallites on the surface, which act as nucleation sites for nanorod growth at later stages [2,27]. The second stage of growth was the deposition of a

ZnO buffer layer using an NaOH-based CBD technique, again described in reference [21]. This process leaves a layer of *c*-axis aligned ZnO nanorods which acts as a buffer layer for subsequent growth of larger nanorods using VPT. Neither the seed nor the buffer layers are isotopically enriched; they have the natural O isotope abundances. Because the PL intensities seen from CBD layers is many orders of magnitude less than that from VPT nanostructures, our PL studies are clearly dominated by emission from the isotopically enriched CTR-VPT grown nanorods, similar to the results seen in our earlier work [21].

The third stage in the growth of ZnO nanorods was CTR-VPT. ZnO powder (60 mg) and graphite powder (60 mg) were carefully mixed to produce a fine homogeneous powder mixture. This powder was then spread over a length of about 2 cm in an alumina boat. The Si wafer was suspended above the powder with the ZnO buffer layer facing downwards towards the powder. The alumina boat was then placed into a quartz tube (inner diameter 37 mm) in a single temperature zone horizontal tube. The exhaust end of the tube was then sealed using a valve. At the other end, a series of valves connect the tube to a vacuum pump, N and O gases and Ar gas via mass flow controllers (MFC). A small regulator was used to control the pressure of the  $^{18}\text{O}_2$  (99%, Sigma Aldrich) lecture bottle. A digital pressure gauge was also present. The tube was slowly evacuated using the vacuum pump to a pressure of  $< 1$  mbar. Following this, the tube was refilled to atmospheric pressure with artificial 'air' that contained  $\sim 21\%$   $^{18}\text{O}_2$  and  $\sim 79\%$   $\text{N}_2$ . Replicating normal atmosphere by only changing the oxygen isotopic mass was important as the VPT growth reaction is known to be sensitive to changes in partial pressures [28]. This mixture was left for about 15 minutes to allow the gasses to mix and fill the entire tube evenly. The Ar flush at 90 sccm was then started, the exhaust valve opened, and after 5 minutes the temperature was raised to  $925^\circ\text{C}$  for 1 hour. The furnace was then allowed to cool for several hours. When the temperature reached about  $350^\circ\text{C}$ , the Ar flow was stopped and the alumina boat removed. This resulted in the growth

of ZnO nanorods aligned with their *c*-axes normal to the substrate, as they grow well aligned on the buffer layer [3].

This CTR-VPT growth process is based on the reduction of ZnO source material by the graphite to produce Zn vapour and carbon monoxide (CO). The Zn vapour is then re-oxidised in a vapour-solid (VS) process at the energetically favourable sites provided by the aligned CBD buffer layer using residual O<sub>2</sub> present in the tube following the Ar flush (rather than the O initially in the ZnO powder, which is captured by C to form CO). In order to grow ZnO nanorods enriched with <sup>18</sup>O isotopes, it was necessary to remove all the residual natural O<sub>2</sub> (i.e. <sup>16</sup>O<sub>2</sub>) from the tube, and then reintroduce <sup>18</sup>O<sub>2</sub> gas as described above.

Three samples were produced using this method: natural Zn<sup>16</sup>O by evacuating the tube and re-filling with <sup>16</sup>O<sub>2</sub> and N<sub>2</sub>, isotopically enriched ZnO by re-filling with <sup>18</sup>O<sub>2</sub> and N<sub>2</sub>, and a mixed 50:50 Zn<sup>16/18</sup>O sample by using a mixture of both oxygen isotopes with N<sub>2</sub>. These samples are labelled as the 'VS' samples.

This method had the disadvantage of requiring significant quantities of isotopically enriched <sup>18</sup>O<sub>2</sub> gas, but was otherwise very successful in terms of achieving growths. In order to confirm that only the residual O<sub>2</sub>, which can be evacuated and replaced with <sup>18</sup>O<sub>2</sub>, contributes to the O in the ZnO nanorods, growth of a nanorod sample was attempted by this method in a pure N<sub>2</sub> atmosphere only. Following this control growth, there was no evidence of VPT nanowire growth at all. Thus, it was confirmed that there is no significant contribution to the VPT growth from O<sub>2</sub> from the ZnO source material, or from older/residual deposited ZnO material on the tube walls from previous growths. This is consistent with previous work in our group that found that the growth process is quenched when the residual O<sub>2</sub> in the tube is sufficiently depleted by a longer Ar flow during the initial steps of the CTR-VPT process, e.g. after about 15-30 minutes Ar flow [29,30].

## 2.2. Vapour-Liquid-Solid VPT method

This method makes use of direct oxidation of Zn metal to effectively “trap” the  $^{18}\text{O}$  to form a  $\text{Zn}^{18}\text{O}$  powder, which could then be used in a vapour-liquid-solid (VLS) VPT growth method. In this case, it is the sublimation of ZnO source powder that provides both the Zn and  $\text{O}_2$  vapours for subsequent growth. Consequently, in order to produce  $^{18}\text{O}$ -enriched ZnO nanorods, it was necessary to produce enriched ZnO source powder. Zn powder (99.9%, Alfa Aesar) was oxidised by placing ~160 mg of such powder in an alumina boat in the furnace and evacuating the tube to  $< 1$  mbar. The tube was then filled with ~200 mbar of either  $^{16}\text{O}_2$  or  $^{18}\text{O}_2$  and ~550 mbar of  $\text{N}_2$  giving a total pressure of ~ 750 mbar, which was experimentally found to be a suitable gas composition to achieve the required oxidation in a reasonable time period at the temperatures used. This mixture was left to settle for about 15 minutes before the furnace was heated to  $800^\circ\text{C}$  for one hour. About 60-90 mg of oxidised powder was recovered from the boat after each run due to some of the produced ZnO depositing on the tube edges. Separate boats and tubes were used for each isotope and smaller tubes of 18 mm internal diameter were used here to reduce the amount of  $^{18}\text{O}_2$  gas needed as it was in limited supply.

$^{18}\text{O}$ -enriched ZnO nanorods were then synthesized using a VLS method with an Au catalyst. The method used was based on previous work on VPT by direct oxidation [31,32]. The setup shows some similarities to that described previously, albeit also with some notable differences. This furnace contained two alumina tubes, one inside the other. Approximately 120 mg of ZnO powder acted as the source material and was spread over about 5-6 cm in an

alumina boat and placed at the centre of the furnace. About 7-8 pieces of Si (100) substrate (~0.5 mm thick and ~1 cm<sup>2</sup> in area) had 10 nm of Au deposited on them by plasma sputter coating and were placed in another alumina boat about 16 cm from the ZnO powder, over a range of a few cm. The tube was sealed and evacuated to a pressure of < 0.3 mbar. The temperature was raised to 1350°C over a period of 5 hours with a pre-determined ramp (400°C for 90 mins, 1150°C for 180 mins, 1350°C for 60 mins). When the temperature reached ~600°C the Ar (99.999%) was introduced at 50 sccm in the reverse direction, i.e. moving any vapour away from the growth substrates. The pressure was held constant at 100 mbar from this point on. After the temperature was at 1350°C for 60 minutes, the growth then took place as the Ar direction was reversed for a further period of 60 minutes and carried the Zn and O<sub>2</sub> vapours downstream from the source powder to the growth substrates. In this VLS method, the Au coating melts and forms catalyst droplets on the substrate which act as energetically favourable nucleation sites. The nanorods in this case are not preferentially aligned due to the absence of a suitable buffer layer. The furnace then cooled down to room temperature before that samples were removed.

Three samples were produced with these oxidised Zn<sup>16</sup>O and Zn<sup>18</sup>O powders: Zn<sup>16</sup>O, Zn<sup>18</sup>O and mixed 50:50 Zn<sup>16/18</sup>O using 60 mg of each powder. The samples produced with this procedure are labelled 'VLS'.

### 2.3. Characterisation

The samples were characterised using scanning electron microscopy (SEM; Carl-Zeiss EVO series, FEI Helios NanoLab 600i), x-ray diffraction (XRD; Bruker AXS D8 Advance Texture Diffractometer), Raman spectroscopy and low temperature PL. Raman measurements were obtained using a Jobin Yvon LabRam HR800 system at room temperature using an Ar laser at 488 nm and an air-cooled CCD detector. PL was carried out using a 325 nm HeCd laser as the excitation source directed onto the sample in a Janis model SHI-950-5 cryostat at ~14 K and a diffraction grating spectrometer system. The spectroscopic system consisted of a 1 m model SPEX 1701 monochromator and Hamamatsu model R3310-02 photomultiplier tube which was cooled to approximately -20 °C. The monochromator contained a grating blazed at 330 nm (ISA model 510-05). A Hg spectral lamp was placed on the optical table such that some of its emission also scattered into the spectrometer entrance slit. The spectral lines from this lamp were used to calibrate the spectra recorded to correct for minor irreproducibility from scan to scan. In addition, the spectra have been corrected for the refractive index of air.

### 3. RESULTS AND DISCUSSION

#### 3.1. Morphology

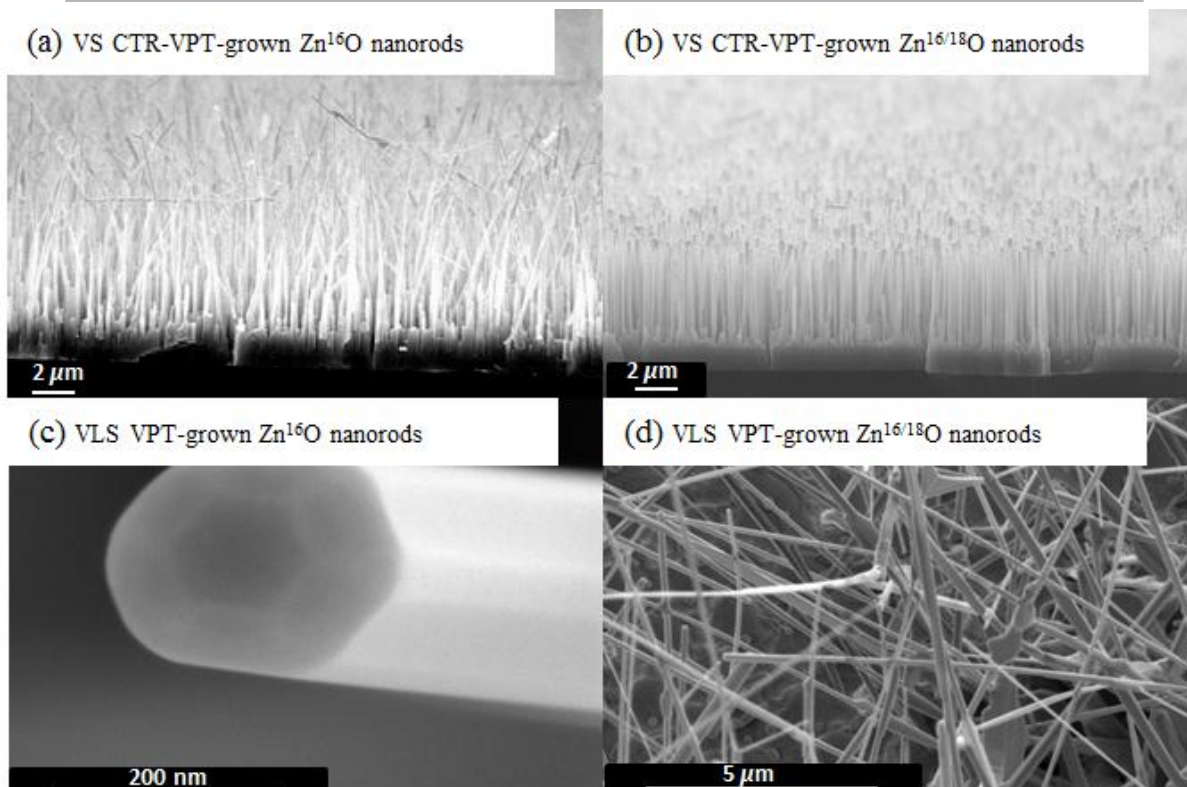


*FIG. 1: SEM images of ZnO nanowires grown via VPT: typical images of samples grown (a,b) via the Modified VS CTR-VPT method and (c,d) using the VLS VPT method. The ZnO nanowires grown with natural abundance are shown in the left column, whereas mixed  $^{16/18}\text{O}$ -enriched are displayed in the right column. No significant differences in the morphology were observed by varying the oxygen species.*

Typical images of the morphology of the VS and VLS samples grown by methods 1 and 2 respectively are shown in figure 1. Figure 1(a) shows the morphology observed in the  $\text{Zn}^{16}\text{O}$ -VS sample and is also typical of the morphology observed in the  $\text{Zn}^{18}\text{O}$ -VS sample, as well as near the edges of the  $\text{Zn}^{16/18}\text{O}$ -VS sample. The nanorods are on the order of  $10\ \mu\text{m}$  in length. They have become entangled, perhaps due to their greater length resulting from a slightly shorter Ar flush time of 5 minutes. Figure 1(b) shows the middle part of the

$\text{Zn}^{16/18}\text{O}$ -VS sample. In this case, the nanorods are a more typical 2-3  $\mu\text{m}$  in length and are more clearly vertically aligned. Note that a slightly longer Ar flush time was used for this sample than for the other VS samples (about 6-7 minutes instead of 5 minutes). This is closer to the usual flush time as used in the Zn-enriched samples previously reported and typical of nanorods grown by our standard VPT growth procedure reported elsewhere [3,21]. This longer Ar flush time results in a smaller amount of residual  $\text{O}_2$  in the tube as the temperature was increased and therefore shorter nanorods due to the growth ceasing when the residual oxygen levels are depleted. This provides a demonstration of just how extremely sensitive the VPT process is to the various parameters, in this case the residual oxygen content during the growth phase. Coverage on these samples was excellent, with the entire sample coated with well aligned ZnO nanorods with high density and structural quality [3,33].

Of the 7-8 pieces of Au-coated Si chips placed in the furnace for these growths, ZnO nanorods were deposited typically on the middle three or four pieces, which were  $\sim 15$  cm from the middle of the ZnO source powder. The temperature here, with values of  $\sim 950$ - $1150^\circ\text{C}$ , was lower than at the centre of the furnace where the source powder was located[31], and this appears to be a key parameter in whether deposits were observed on a particular piece, because the pieces were spread over a distance of a few cm.

Figure 1(c) and (d) display the typical morphology observed of the VLS samples grown using the VLS VPT method. Figure 1(c) shows a close up of the end of a nanorod of  $\text{Zn}^{16}\text{O}$ -VLS clearly showing the hexagonal crystal structure associated with wurtzite structure. Figure 1(d) shows the  $\text{Zn}^{16/18}\text{O}$ -VLS sample. The VLS nanorods are generally longer than those grown by VS, with lengths of several tens of  $\mu\text{m}$  observed in all samples. The diameters of several individual nanorods were measured with values in the range of  $\sim 100$ - $220$  nm, with most being between 120-150 nm. These dimensions agree with the

ranges previously reported using this growth technique [31,34]. The greatest difference in ensemble morphology between these VLS samples and those grown with the VS method is that there is no preferential alignment of the  $c$ -axes of the nanorods with respect to the substrate. This is because of the lack of an epitaxially matched  $c$ -axis aligned buffer layer in the case of the VLS growth. Coverage on the substrates with deposits was excellent, with the entire surface displaying this high density nanorod growth.

### 3.2. Alignment and Crystal Quality

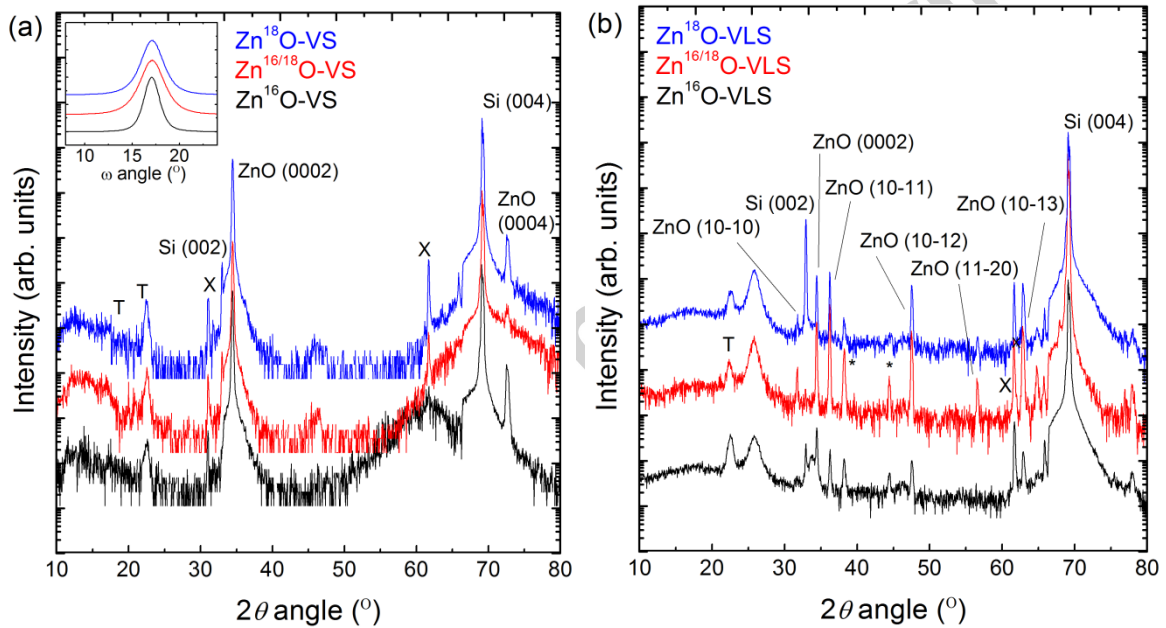


FIG. 2: X-ray  $2\theta$ - $\omega$  diffractograms of the (a) VS samples dominated by the Si substrate peak at  $69.1^\circ$  and the ZnO peak at  $34.4^\circ$ , and (b) VLS samples dominated by the Si substrate peak at  $69.1^\circ$  and containing multiple ZnO peaks (assigned in the graph), as the ZnO nanorods are not aligned in respect to the sample surface. Inset in (a) shows rocking curves of the respective ZnO (0002) peaks (the  $\text{Zn}^{16}\text{O}$  curve was shifted to align with the others as described in the text).

Figure 2(a) shows the  $2\theta$ - $\omega$  XRD scans of the VS samples grown using the Modified VS CTR-VPT method. The diffractograms are similar to those typically obtained from natural and Zn-enriched  $c$ -axis aligned nanorods [21,35]. The diffractograms are dominated by the ZnO (0002) reflection at  $\sim 34.4^\circ$  and the Si (004) substrate reflection at  $\sim 69.1^\circ$ . The second order ZnO (0004) reflection and the forbidden Si (002) reflection [36] are also present. Some features associated with  $K\beta$  contamination from the x-ray tube, as well as features not related to the ZnO nanorods and associated with the backing tape used to mount the samples [37] are marked X and T, respectively. The strong reflection at  $\sim 34.4^\circ$  indicates successful deposition of wurtzite ZnO on the substrate. Their narrow values of FWHM ( $< 0.2^\circ$ ) indicate high crystal quality in terms of out-of-plane coherence lengths/nanocrystallite sizes. The inset shows the rocking curves of the ZnO (0002) reflection. The high quality of the ZnO crystal structure, and the high degree of preferential vertical alignment along the  $c$ -axis, is demonstrated by the narrow line widths of the rocking curves ( $1.96$ - $3.08^\circ$ ). These data are consistent with the SEM images of these samples. The peak position of the  $\text{Zn}^{16}\text{O}$ -VS rocking curve was slightly shifted by  $\sim 1^\circ$  to a lower energy due to a variation in the mechanical tilt of this sample during mounting on the instrument stage [35]. It was shifted artificially when plotted to align with the other samples in this set (at half the value of the  $2\theta$  peak maximum).

Figure 2(b) shows the corresponding  $2\theta$ - $\omega$  diffractograms for the VLS samples grown using the VLS VPT method. The diffractograms have a distinctly different appearance to those previously observed in the VS and other samples with their  $c$ -axes aligned vertically [35]. The diffractograms are dominated by the Si (004) reflection of the substrate, and the Si (002) reflection is again present. However, instead of being dominated by the ZnO (0002)

reflection at  $34.4^\circ$  indicating *c*-axis aligned wurtzite ZnO, there are a number of peaks associated with different planes in wurtzite ZnO present. These include the *c*-plane (0002), the *m*-plane (10-10), the *s*-plane (10-11), the *r*-plane (10-12), the *a*-plane (11-20) and the (10-13) reflection [38]. The presence of such a number of different ZnO planes in the  $2\theta$ - $\omega$  spectrum is in agreement with the fact that the material is not preferentially aligned. Each nanorod exhibits a different orientation to its neighbours, and so there are some nanorods in the appropriate orientation for each of these planes to appear as their reflections satisfy the Bragg equation, i.e. an approximation to the powder pattern is seen. These measurements are consistent with the SEM images of these samples which show nanorods have grown in all directions without any preferential alignment of their *c*-axes in the vertical direction. The peak at  $\sim 25^\circ$  in figure 2(b) is assigned to quartz/glass due to high temperature oxidation of Si substrate in the VLS system [39]. Additionally, the peaks marked \*, at  $\sim 39^\circ$  and  $\sim 45^\circ$ , are unidentified and we suggest they could be due to an interfacial layer of  $\text{Zn}_2\text{SiO}_4$  [33].

The *c* lattice constants were calculated using the Bragg formula for both the VS and VLS samples, and the *c* lattice constant agrees with the expected (bulk crystalline) value of 0.521 nm in all samples [40].

### 3.3. Phonon Frequencies and Enrichment

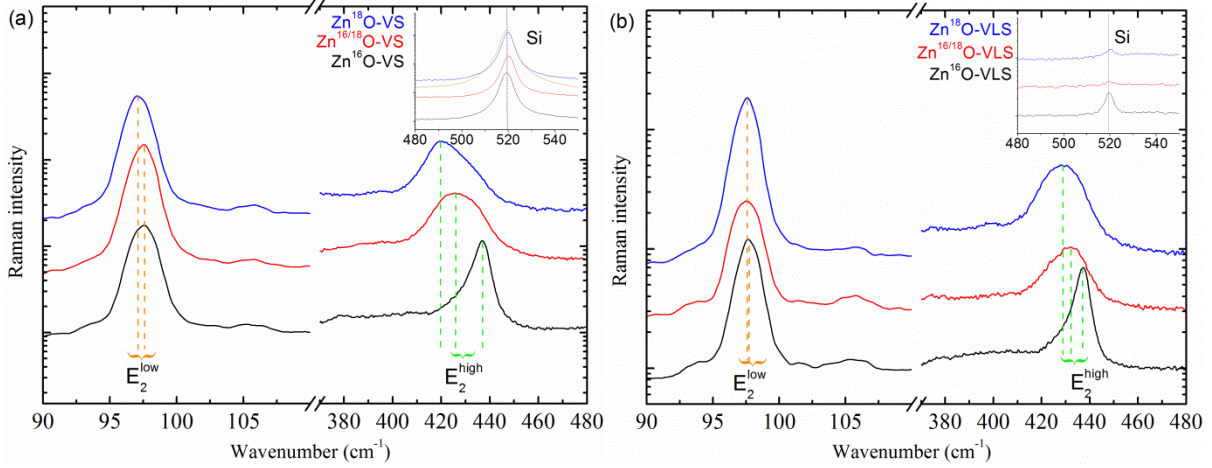


FIG. 3: Raman spectra of the (a) VS, and (b) VLS, O-enriched ZnO nanorods as a function of enrichment. The inset shows the respective signal from the Si substrate from the same spectra, which remained unchanged.

Raman spectroscopy was performed focussing on the  $E_2^{\text{high}}$  and  $E_2^{\text{low}}$  phonon modes of the ZnO material [41]. Figure 3 shows these Raman spectra for the (a) VS and (b) VLS grown nanorod ensembles. Table 1 gives the phonon line frequencies, their FWHM, and the differences in these from the  $\text{Zn}^{16}\text{O}$  sample in each case. Changing the isotope from  $^{16}\text{O}$  to  $^{18}\text{O}$ , the  $E_2^{\text{high}}$  mode of ZnO induces a shift of  $16.51\text{ cm}^{-1}$  in the VS grown sample set and  $8.42\text{ cm}^{-1}$  in the VLS set. These figures are much larger than the  $2.17\text{ cm}^{-1}$  shift reported when changing the Zn isotope from  $^{64}\text{Zn}$  to  $^{68}\text{Zn}$  in Zn-enriched nanorods [21]. This is not surprising as this mode is dominated by the O atom vibration/movement [42] and therefore we would expect a larger change when changing the O isotope than the Zn. The relative change in atomic mass is also much greater for O (11% for O and 6% for Zn). Shifts of  $\sim 21\text{ cm}^{-1}$  at low temperatures [43] and  $\sim 23\text{ cm}^{-1}$  at room temperatures [44] have been reported by Serrano *et al.* The widths of these lines, in the samples with  $^{18}\text{O}$  included, are much larger than those observed for Zn enrichment, in some cases three times larger. Serrano *et al.* also

observed this increase in line widths, and attributed the change in line widths in the isotopically pure samples to the ‘ridge’ in the two-phonon density of states in this region. The changing O masses shift the phonon frequencies along this ridge, which itself only depends on the Zn mass in the region of  $E_2^{\text{high}}$  which they studied. There is an additional broadening effect for the mixed  $\text{Zn}^{16/18}\text{O}$  samples, which they attribute to additional elastic scattering of phonons due to the O isotopic variations and a reduction in phonon lifetime as a result, and they observed this sample to have the widest line. It is noted that although the broad trends are in agreement with these reports, the widths recorded here are larger than those reported by Serrano *et al*, who observed an increase in the widths of these lines from  $6 \text{ cm}^{-1}$  to  $11 \text{ cm}^{-1}$  moving from  $\text{Zn}^{16}\text{O}$  to  $\text{Zn}^{18}\text{O}$  at room temperature [44]. We observe such changes from  $6 \text{ cm}^{-1}$  to  $16 \text{ cm}^{-1}$ , and  $6 \text{ cm}^{-1}$  to  $18 \text{ cm}^{-1}$ , in the VS and VLS samples respectively. In addition, for the VLS samples, the  $\text{Zn}^{18}\text{O}$ -VLS sample is the widest, not the  $\text{Zn}^{16/18}\text{O}$ -VLS sample. The larger widths observed for the lines from the  $\text{Zn}^{18}\text{O}$  samples may indicate lower levels of isotopic enrichment, as explored further below, and may also be associated in part with some degree of inhomogeneity of isotopic enrichment over both individual nanorods and the nanorod ensemble.

By contrast the  $E_2^{\text{low}}$  mode experiences very little change as this mode is Zn-dominated [42]. The shifts of  $0.37 \text{ cm}^{-1}$  and  $0.14 \text{ cm}^{-1}$  are much smaller than the  $1.81 \text{ cm}^{-1}$  shift reported for this mode in Zn-enriched ZnO nanorod samples [21]. This mode also remains quite narrow and has only small changes in width, although larger than the changes in width due to Zn isotope changes.

While the Raman spectra indicate, based on the  $E_2^{\text{high}}$  mode frequency shifts, that O-isotopic enrichment has been successful in both sets, it appears to indicate a lower level of enrichment than expected (based on the nominal enrichments). Additionally, the VLS

samples have been enriched to a lesser extent than the VS samples, resulting in smaller  $E_2^{\text{high}}$  mode Raman shifts. This is consistent with the PL data presented in the next section. The wider line widths in our samples, and in particular our  $\text{Zn}^{18}\text{O}$ -VLS sample which had a wider line than the  $\text{Zn}^{16/18}\text{O}$ -VLS samples, also indicate that  $^{18}\text{O}$ -enrichment is lower than anticipated.

Table 1: Frequencies and FWHM of the  $E_2^{\text{low}}$  and  $E_2^{\text{high}}$  phonons for the VS and VLS O-enriched nanowire samples.

Sample	Mode	Wavenumber ( $\text{cm}^{-1}$ )	$\Delta$ Wavenumber ( $\text{cm}^{-1}$ )	FWHM ( $\text{cm}^{-1}$ )	$\Delta$ FWHM ( $\text{cm}^{-1}$ )
VS samples					
$\text{Zn}^{16}\text{O}$ -VS	$E_2^{\text{high}}$	436.85	-	6.73	-
$\text{Zn}^{16/18}\text{O}$ -VS	$E_2^{\text{high}}$	426.25	-10.6	20	13.27

Zn <sup>18</sup> O-VS	E <sub>2</sub> <sup>high</sup>	420.34	-16.51	16.37	9.64
Zn <sup>16</sup> O-VS	E <sub>2</sub> <sup>low</sup>	97.51	-	2.1	-
Zn <sup>16/18</sup> O-VS	E <sub>2</sub> <sup>low</sup>	97.52	0.01	1.93	-0.17
Zn <sup>18</sup> O-VS	E <sub>2</sub> <sup>low</sup>	97.14	-0.37	1.96	-0.14
VLS samples					
Zn <sup>16</sup> O-VLS	E <sub>2</sub> <sup>high</sup>	437.32	-	6.35	-
Zn <sup>16/18</sup> O-VLS	E <sub>2</sub> <sup>high</sup>	432.07	-5.25	16.27	9.92
Zn <sup>18</sup> O-VLS	E <sub>2</sub> <sup>high</sup>	428.9	-8.42	18.54	12.19
Zn <sup>16</sup> O-VLS	E <sub>2</sub> <sup>low</sup>	97.71	-	1.76	-
Zn <sup>16/18</sup> O-VLS	E <sub>2</sub> <sup>low</sup>	97.54	-0.17	2.32	0.56
Zn <sup>18</sup> O-VLS	E <sub>2</sub> <sup>low</sup>	97.57	-0.14	1.81	0.05

### 3.4. Optical Quality and Enrichment

The PL spectra contain a strong band edge emission and varying intensities of deep level emission in the visible spectral region. Figure 4 shows the band edge spectra in detail for both (a) the VS samples and (b) the VLS samples. The main features are the In-related I<sub>9</sub> line (attributed to impurities in the ZnO powder source material) and the Al-related I<sub>6</sub> line of ZnO (attributed to the alumina boat [45–47]). Other prominent features which appear include

the SX feature[48] which is present in some of the VS samples and the ionised In donor-related  $I_2$  line[49] and ionised Al donor-related  $I_0$  line[50] which are present in the VLS samples. The position of the  $I_9$  In-related bound exciton (BX) recombination in unenriched material at  $\sim 3.356$  eV was used to measure changes in the band edge positions with changing O isotope enrichment, and all the other PL-lines followed the trend of this feature. The positions of the  $I_9$  line in each sample are given in table 2, along with their FWHM. There is a monotonic increase in emission energy as the O isotopic mass changes from natural  $^{16}\text{O}$  to  $^{18}\text{O}$ . This blue shift is  $\sim 3.24$  meV in the VS sample set, and  $\sim 2.11$  meV for the VLS samples. The changing positions of the band edge BX lines are strong evidence of successful isotopic enrichment of the samples. Manjón *et al.* have reported shifts of the BX recombinations of  $\sim 6.4$  meV over this range [19]. In addition, Tsoi *et al.* have reported a similar shift of  $\sim 6.5$  meV in the A-exciton band gap over this range [20]. Both of these measurements used single crystal ZnO samples, rather than ZnO nanostructures. The  $\text{Zn}^{16/18}\text{O}$  line energies also appear slightly closer to  $\text{Zn}^{18}\text{O}$  than  $\text{Zn}^{16}\text{O}$ , i.e. the shift with isotopic mass may be slightly nonlinear. This also is consistent with data reported by Manjón *et al.* [19]. The other I-lines in our samples follow the same shift pattern as the  $I_9$  line. The features observed in both the VS and VLS samples were similar to those previously reported for Zn-enriched ZnO nanorods using a similar VPT growth method [21].

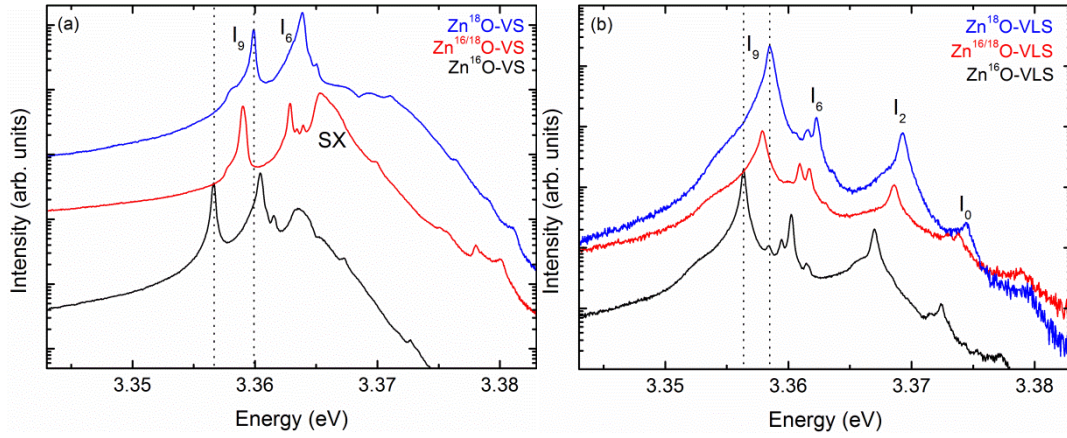


FIG 4: Band edge region of the low-temperature (14 K) PL spectra in the (a) VS and (b) VLS O-enriched nanorod samples as a function of enrichment. (Spectra offset vertically for clarity.)

Table 2: Peak positions and FWHM of the I<sub>9</sub> exciton recombination in the VS and VLS O-enriched samples.

Sample	I <sub>9</sub> energy (eV)	I <sub>9</sub> FWHM (meV)
Zn <sup>16</sup> O-VS	3.35662	0.35
Zn <sup>16/18</sup> O-VS	3.35903	0.48
Zn <sup>18</sup> O-VS	3.35986	0.34
Zn <sup>16</sup> O-VLS	3.35635	0.41
Zn <sup>16/18</sup> O-VLS	3.35783	0.67

---

Zn <sup>18</sup> O-VLS	3.35846	0.80
------------------------	---------	------

---

As these previously reported shifts are larger than those in our samples, this again appears to indicate a lower level of enrichment than expected, and additionally that the VLS samples have been enriched to a lesser extent than the VS samples. This is consistent with the reduced  $E_2^{\text{high}}$  phonon frequency changes observed in Raman studies on these samples reported above. The line widths of the BX lines in our VS and VLS samples are very narrow ( $< 1$  meV) and specifically much narrower than those previously reported by Manjón *et al.* ( $< 5$  meV) and Tsoi *et al.* (2-8 meV) in their isotopically enriched bulk single crystal samples. We note however that our sample still show appreciable residual line broadening, possibly due to inhomogeneous strain or other effects. Despite this, the very narrow line widths in our nanostructured VS and VLS samples clearly demonstrate their excellent optical quality and potential for use in detailed optical studies of defects and impurities using low temperature PL, and indeed on individual nanorods using  $\mu$ PL [51].

### 3.5 Estimate of Level of Enrichment in O-enriched ZnO

An estimate of the level of enrichment achieved in our samples was made by comparing our band edge region BX energy shifts to those reported by Manjón *et al.* and Tsoi *et al.* [19,20]. Moving from Zn<sup>16</sup>O to Zn<sup>18</sup>O, the average shift in those two reports is  $\sim 6.45$  meV. Using this as a reference and given a linear dependence, we then calculate the shifts observed in the band edge region in our VS and VLS samples as a percentage of this, for both

the Zn<sup>18</sup>O and the Zn<sup>16/18</sup>O mixed isotope samples. The assumption of a linear behaviour is reasonable in light of previous data from Manjón *et al.*[19], in terms of providing an estimate of the enrichment to an accuracy of ~10% which is the scale of the error in this approximation based on the data from Manjón *et al* [19]. The same calculation can also be carried out using the E<sub>2</sub><sup>high</sup> phonon energy shifts compared to the room temperature value of ~23 cm<sup>-1</sup> reported by Serrano *et al* [44]. Across the PL and Raman data, this gives an average estimated <sup>18</sup>O enrichment of 60% for Zn<sup>18</sup>O-VS, 35% for Zn<sup>18</sup>O-VLS, 40% for Zn<sup>16/18</sup>O-VS and 25% for Zn<sup>16/18</sup>O-VLS, with an error of ±5% in all cases.

### 3.6 Discussion on Possible Causes of Reduced Oxygen Enrichment

During both the growth of the VS samples by the Modified VS CTR-VPT method, and the oxidation of the Zn metal powders to produce the ZnO source powders for the VLS growths by the VLS VPT method, every effort was made to ensure that only the appropriate O isotope was present in the furnace tube.

Considering firstly the Modified VS CTR-VPT method; for the growth of <sup>18</sup>O-enriched ZnO nanorods by this method, involving evacuating the furnace tube and refilling with <sup>18</sup>O<sub>2</sub>, we must consider any possible sources of natural <sup>16</sup>O<sub>2</sub> as a contaminant, which could lead to reduced <sup>18</sup>O enrichment as observed in these samples. One obvious source of this is the natural <sup>16</sup>O<sub>2</sub> in the tube at the start of the experiment. The tube was evacuated to a pressure of <1 mbar and subsequently filled to 21% atmospheric pressure with <sup>18</sup>O<sub>2</sub> and the remaining 79% atmospheric pressure with N<sub>2</sub>. This would indicate a possible contamination level of ~0.1% <sup>16</sup>O<sub>2</sub>, or ~0.5% of the oxygen being this isotope. This certainly would not

explain the enrichment being reduced by approximately one half as indicated by the PL data. The  $N_2$  used in the experiment only has  $O_2$  impurities of  $< 5$  ppm, or around 0.0005%. Clearly this could not be the source of such reduced enrichment in the atmosphere inside the tube during growth. The system was extensively checked for leaks several times during the setup and the lines were purged of natural  $^{16}O_2$  before growth including the regulator used on the  $^{18}O_2$  cylinder. The natural  $^{16}O$  in the ZnO source powder (or the small amounts likely to be adsorbed on the graphite powder) is also not the cause of this effect, because the CTR reaction leads to the formation of CO molecules, thereby trapping the O in the ZnO source powder and not allowing it to react on the substrate, as the residual atmospheric  $O_2$  does. Attempts at growth with just  $N_2$  gas in the tube mentioned previously, and the lack of observed growth from such attempts, strongly support this conclusion concerning the VS growth mechanism in the Modified VS CTR-VPT method being associated with residual oxygen rather than the oxygen from the ZnO source powder.

We also considered whether ZnO residue on the inside of the furnace tube (or some remaining in the alumina boat) from previous growths, or from the buffer layers, could contribute some  $^{16}O_2$  gas to the growth environment by a small amount of it being disassociated when heated, because the  $^{18}O$ -enriched VS growths were carried out in the same tube as the normal natural isotope growths and the buffer layers are not isotopically enriched with  $^{18}O$ . However, based on an analysis of the system energetics for direct dissociation of ZnO without CTR, the temperatures of  $925^\circ C$  are not sufficient for this to occur to any significant extent. We emphasise again that no VPT growth occurred when the system was tested using a pure  $N_2$  atmosphere with no  $O_2$  gas of any kind introduced, indicating that leaks or another unwanted sources of  $^{16}O_2$  gas in the system, e.g. via dissociation of tube/boat materials, residues from previous growths or buffer layers, are not

the cause of the poorer enrichment. We now consider the VLS sample growths. The system used to oxidise the Zn metal powder, using  $^{16}\text{O}_2$  or  $^{18}\text{O}_2$ , to produce  $\text{Zn}^{16}\text{O}$  and  $\text{Zn}^{18}\text{O}$  powders to be used in these growths was similar to the VS system and therefore much of discussion in the previous paragraph also applies to this method. In this case, a smaller tube was used to reduce the amount of gas needed. Additionally, a separate clean tube and boat was used for the  $^{18}\text{O}$  isotope oxidation, to eliminate possible contamination. This, coupled with the lower oxidation temperatures of  $\sim 800^\circ\text{C}$ , means we can be quite confident of having little or no contamination here. Completely fresh Zn metal powder was used for the  $^{18}\text{O}$  oxidation runs. It is considered likely that the cause of the even further reduced enrichment in the VLS samples compared to the VS samples is that this second growth system led to increased  $^{16}\text{O}$  contamination. These growths were carried out using an alumina boat and tube that had deposits from previous growths present. This residue is considered the likely source of additional  $^{16}\text{O}_2$  in the tube due to the higher temperatures ( $\sim 1350^\circ\text{C}$ ) used in this system for the sublimation of the ZnO sources powders, which will also cause sublimation from the previous deposits, producing some  $^{16}\text{O}_2$  contamination.

Finally, a number of further experiments were carried out in an attempt to clarify the source of the  $^{16}\text{O}$  contamination of these samples. Firstly, a further sample of  $\text{Zn}^{18}\text{O}$ -VS was grown using the same CTR-VPT method except with a bottle of  $^{18}\text{O}_2$  gas sourced from a different supplier (CK Isotopes, 98%). The PL spectrum showed a band edge shift of 3.12 meV for the  $I_9$  line for a nominally 100%  $\text{Zn}^{18}\text{O}$  sample, similar to those recorded with the initially grown  $\text{Zn}^{18}\text{O}$  VS sample. Secondly, the same growth was repeated using a fresh tube and alumina boat, which had no deposits from previous unenriched growths. The results here were a band edge shift of 3.45 meV for the  $I_9$  line which indicates that there is no contamination from old deposits on the equipment. Finally, a further VPT experiment was

carried out using a long 1 hour Ar flush at the start (versus the usual ~ 5 mins). This removes all the residual oxygen from the tube and should result in no VPT nanorod growth. Indeed, this is what was observed. This implies no other source of  $^{16}\text{O}_2$  in the system and is consistent with the  $\text{N}_2$  only test described earlier and with tests by others using this system [30].

Based on the entirety of the evidence above, it would appear that the source of  $^{16}\text{O}$  contamination must come from sources of oxygen already chemically bound within the growth system (rather than  $^{16}\text{O}_2$  gas) which can move into the growing nanorods, by a process of exchange with the  $^{18}\text{O}$  in the gas phase. In this regard we discuss three possible mechanisms below.

Firstly, there may be significant diffusion/migration of  $^{16}\text{O}$  from the unenriched CBD buffer layer in the case of the VS samples, into the nanorods after they form during the high temperature growth period. This particular mechanism is not applicable to the VLS samples since the  $\text{SiO}_2$  native oxide layer on the Si surface is too thin (2-3 nm) to supply a sufficient number of  $^{16}\text{O}$  atoms. It is unlikely that bulk diffusion of  $^{16}\text{O}$  is responsible; diffusion constants available in the literature predict diffusion lengths  $2\sqrt{D \cdot t}$ , where  $D$  is the diffusion constant and  $t$  the growth time, which are typically less than ~10 nm for the growth conditions used in our work in the case of both VS and VLS growths [52]. Given the nanorod lengths in the present work ( $> 1 \mu\text{m}$  in all cases) this bulk diffusion mechanism does not explain our results. However it is well known that the surface of ZnO is a chemically very active environment and oxygen exchange between bulk oxygen, mobile surface chemisorbed oxygen and gas phase oxygen can readily occur at elevated temperatures [53]. Significantly enhanced diffusion/migration along the free nanorod sidewalls may be possible by virtue of the surface chemisorbed oxygen, compared to diffusion in single crystals. Indeed

significantly enhanced diffusion effects have already been reported at grain boundaries in ZnO [54]. Given the large surface to volume ratio of the nanorod morphology, this type of effect would be expected to be much more important for nanorods than for bulk crystals or thin films. The formation and growth of the nanorods requires the reaction of Zn and O<sub>2</sub> in the gas phase at the substrate surface, but subsequently there may be significant surface diffusion/migration of oxygen between the substrate and nanorods during the high temperature growth period leading to the loss of <sup>18</sup>O enrichment we observe in the final grown nanorods. The fact that similar loss of isotopic enrichment was not seen in our Zn isotopically enriched nanorods reported previously, despite the larger bulk diffusion coefficient for Zn in ZnO, is also consistent with this surface diffusion/migration mechanism, since oxygen is known to be the main surface chemisorbed native species on ZnO surfaces [21,52]. This mechanism is consistent with effects observed in the CBD layer when they underwent a growth cycle which resulted in no VPT growth (i.e. with only N<sub>2</sub> in the tube or after a long Ar flush), where significant changes in morphology are seen which may be due to oxygen surface diffusion/migration, as illustrated in figure 5. The planned  $\mu$ Raman and  $\mu$ PL measurements on single nanorods mentioned previously may enable us to determine the influence of such an effect, by observing changes in peak energies along a single nanorod associated with a gradient in isotopic enrichment.

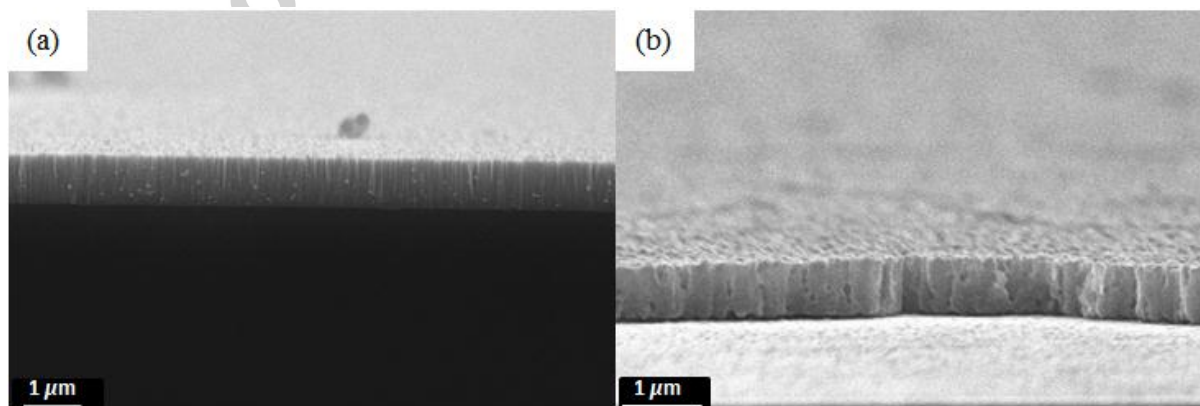


*FIG 5: SEM image of typical buffer layer of CBD-grown ZnO nanorods (a) before and (b) after the VPT cycle in an oxygen-depleted atmosphere. No VPT growth occurs and changes in morphology are observed.*

Secondly, there may be exchange of  $^{18}\text{O}$  with  $^{16}\text{O}$  in the polycrystalline quartz/alumina tubes/boats at high temperature, a mechanism relevant to both the VS and VLS samples. Although both the quartz and alumina materials are stable with respect to thermal decomposition (thermolysis) at the temperatures used, there is no difference in initial and final state energies for a process of oxygen interchange between the solid and gas unlike the situation for thermolysis (or only a small one of the order of meV due to the isotopic differences' effect on vibronic levels), so the equilibrium constant should be close to one. Clearly there will be an activation energy associated with oxygen interchange, but the surfaces of such polycrystalline oxides are known to be active regions for oxygen adsorption/chemisorption and interchange with the surface and immediate sub-surface layers, via oxygen vacancy sites or similar and this might reduce the activation energy to a degree where the process can proceed at the relevant growth temperatures [53]. The oxide surface area of the tubes and boats is very large due to the size and polycrystalline nature of these, so if such a process (with negligible difference in initial and final state energies) did proceed, it might well allow enough interchange to produce the  $^{16}\text{O}$  contamination we see. This interchange could only happen if there is  $\text{O}_2$  gas in the tube, consistent with our observations of no growth in  $\text{N}_2$  only. We note that reasonably efficient ionic interchange between a liquid and ZnO surface has previously been observed by our group and others, albeit for the case of a metal cation [55,56].

Finally, and rather similar to the second mechanism proposed above and likely to operate in parallel, all surfaces tend to have a layer of adsorbed water of the order of a few monolayers thickness (and the polycrystalline oxide tube and boat materials have large surfaces). This generally requires pumping at high temperatures under ultra-high vacuum to be removed, which was not possible in our growth systems. Exchange of  $^{18}\text{O}$  with  $^{16}\text{O}$  with this adsorbed water layer could act as a source of  $^{16}\text{O}$  contamination, a mechanism again relevant to both the VS and VLS samples and once again this interchange could only happen if there is  $\text{O}_2$  gas in the tube, consistent with our observations of no growth in  $\text{N}_2$  only. For the same reasons as stated in respect of the second mechanism above, exchange of  $^{18}\text{O}$  with  $^{16}\text{O}$ , rather than thermolysis of the water molecules, is more likely with the activation energy for the exchange possibly reduced by the interaction of the water molecules with the polycrystalline oxide surfaces of the tubes/boats, since it is known that oxide surfaces interact strongly with water molecules, leading to effects such as dissociative adsorption [57].

The three proposed mechanisms are presently speculations on our part. They are however all consistent with the observed experimental data and are physically reasonable hypotheses. Further experimentation will be required to determine the extent of involvement of each mechanism in our system and specifically  $\mu\text{Raman}$  and  $\mu\text{PL}$  measurements on single nanorods are currently being planned to investigate the first mechanism.

#### 4. CONCLUSION

We have developed two novel methods to grow ZnO nanorod samples isotopically enriched with  $^{18}\text{O}$ . Firstly, the previously developed three-step process used to grow natural

and Zn-enriched ZnO nanorods has been further modified, by replacing the atmospheric O<sub>2</sub> with enriched <sup>18</sup>O<sub>2</sub>, in order to grow O-enriched ZnO nanorods using this VS method on CBD buffer layers. In addition, O-enriched ZnO nanorods were successfully grown using isotopically enriched source powders in a separate VLS growth system. SEM studies confirmed the success of both growth methods in terms of nanorod growth, although in the case of the VLS samples, the nanorods were not aligned with their *c*-axes perpendicular to the sample surface due to the non-epitaxial relation of nanorods with the substrate. Raman and PL studies clearly indicated that O-enrichment was successful in both cases, although the results show the enrichment is at a lower level in our samples compared to previous reports with the same nominal enrichment levels. The very narrow PL line widths, far narrower than those reported previously in the literature for isotopically enriched bulk ZnO, in our VS and VLS samples demonstrate their excellent optical quality and their potential for use in detailed optical studies of defects and impurities using low temperature PL.

The origin of the reduced enrichment level is most likely due to sources of oxygen already chemically bound within the growth system which can move into the growing nanorods, by some process of exchange with the <sup>18</sup>O, with some additional contribution of <sup>16</sup>O from ZnO residue on the tube and boat in the case of the VLS samples due to the higher temperatures used in that method. We have proposed three mechanisms which are all consistent with the observed experimental data and are physically reasonable hypotheses but further experimentation will be required to determine the extent of involvement of each mechanism in the used growth system.

#### ACKNOWLEDGEMENTS

CG acknowledges Dr. Rajani Vijayaraghavan for her assistance with the Raman measurements in DCU. CG and EMcG gratefully acknowledge funding for this work from the Irish Research Council (IRC) under an EMBARK Initiative postgraduate scholarship. This work was financially supported by the Deutsche Forschungsgemeinschaft (DFG) within the frame of FOR1616.

## REFERENCES

- [1] D. Bao, H. Gu, A. Kuang, Sol-gel-derived c-axis oriented ZnO thin films, *Thin Solid Films*. 312 (1997) 37–39. doi:10.1016/S0040-6090(97)00302-7.
- [2] L.E. Greene, M. Law, D.H. Tan, M. Montano, J. Goldberger, G. Somorjai, et al., General Route to Vertical ZnO Nanowire Arrays Using Textured ZnO Seeds, *Nano Lett.* 5 (2005) 1231–1236. doi:10.1021/nl050788p.
- [3] D. Byrne, E. McGlynn, K. Kumar, M. Biswas, M.O. Henry, G. Hughes, A Study of Drop-Coated and Chemical Bath-Deposited Buffer Layers for Vapor Phase Deposition of Large Area, Aligned, Zinc Oxide Nanorod Arrays, *Cryst. Growth Des.* 10 (2010) 2400–2408. doi:10.1021/cg100231u.
- [4] S.H. Jo, J.Y. Lao, Z.F. Ren, R.A. Farrer, T. Baldacchini, J.T. Fourkas, Field-emission studies on thin films of zinc oxide nanowires, *Appl. Phys. Lett.* 83 (2003) 4821. doi:10.1063/1.1631735.
- [5] M. Law, L.E. Greene, J.C. Johnson, R. Saykally, P. Yang, Nanowire dye-sensitized solar cells., *Nat. Mater.* 4 (2005) 455–9. doi:10.1038/nmat1387.

- [6] J. Grabowska, A. Meaney, K. Nanda, J.-P. Mosnier, M. Henry, J.-R. Duclère, et al., Surface excitonic emission and quenching effects in ZnO nanowire/nanowall systems: Limiting effects on device potential, *Phys. Rev. B.* 71 (2005) 115439. doi:10.1103/PhysRevB.71.115439.
- [7] T. Long, S. Yin, K. Takabatake, P. Zhnag, T. Sato, Synthesis and Characterization of ZnO Nanorods and Nanodisks from Zinc Chloride Aqueous Solution., *Nanoscale Res. Lett.* 4 (2009) 247–253. doi:10.1007/s11671-008-9233-2.
- [8] X.Y. Kong, Z.L. Wang, Spontaneous Polarization-Induced Nanohelices, Nanosprings, and Nanorings of Piezoelectric Nanobelts, *Nano Lett.* 3 (2003) 1625–1631. doi:10.1021/nl034463p.
- [9] Y. Wang, X. Chen, J. Zhang, Z. Sun, Y. Li, K. Zhang, et al., Fabrication of surface-patterned and free-standing ZnO nanobowls, *Colloids Surfaces A Physicochem. Eng. Asp.* 329 (2008) 184–189. doi:10.1016/j.colsurfa.2008.07.018.
- [10] Z. Fan, P. Chang, J.G. Lu, E.C. Walter, R.M. Penner, C. Lin, et al., Photoluminescence and polarized photodetection of single ZnO nanowires, *Appl. Phys. Lett.* 85 (2004) 6128. doi:10.1063/1.1841453.
- [11] J. Bao, M.A. Zimmler, F. Capasso, X. Wang, Z.F. Ren, Broadband ZnO Single-Nanowire Light-Emitting Diode, *Nano Lett.* 6 (2006) 1719–1722. doi:10.1021/nl061080t.
- [12] R. Röder, T.P.H. Sidiropoulos, R. Buschlinger, M. Riediger, U. Peschel, R.F. Oulton, et al., Mode Switching and Filtering in Nanowire Lasers, *Nano Lett.* 16 (2016) 2878–2884. doi:10.1021/acs.nanolett.6b00811.

- [13] G. Davies, E.C. Lightowers, R. Woolley, R.C. Newman, a S. Oates, Carbon in radiation damage centres in Czochralski silicon, *J. Phys. C Solid State Phys.* 17 (1984) L499–L503. doi:10.1088/0022-3719/17/19/005.
- [14] M.L.W. Thewalt, Spectroscopy of excitons and shallow impurities in isotopically enriched silicon—electronic properties beyond the virtual crystal approximation, *Solid State Commun.* 133 (2005) 715–725. doi:10.1016/j.ssc.2004.12.023.
- [15] D. Barba, D. Koshel, F. Martin, G.G. Ross, M. Chicoine, F. Schiettekatte, et al., Silicon nanocrystal synthesis by implantation of natural Si isotopes, *J. Lumin.* 130 (2010) 669–673. doi:10.1016/j.jlumin.2009.11.014.
- [16] F.J. Manjón, M. a. Hernández-Fenollosa, B. Marí, S.F. Li, C.D. Poweleit, a. Bell, et al., Effect of N isotopic mass on the photoluminescence and cathodoluminescence spectra of gallium nitride, *Eur. Phys. J. B.* 40 (2004) 453–458. doi:10.1140/epjb/e2004-00211-1.
- [17] J.M. Zhang, T. Ruf, M. Cardona, O. Ambacher, M. Stutzmann, J.-M. Wagner, et al., Raman spectra of isotopic GaN, *Phys. Rev. B.* 56 (1997) 14399. doi:10.1103/PhysRevB.56.14399.
- [18] T. Meyer, D. Karaiskaj, M.L. Thewalt, M. Cardona, Effect of the isotopic mass of gallium on the indirect gap of GaP, *Solid State Commun.* 126 (2003) 119–123. doi:10.1016/S0038-1098(03)00030-9.
- [19] F.J. Manjón, M. Mollar, M.A. Hernández-Fenollosa, B. Marí, R. Lauck, M. Cardona, Effect of isotopic mass on the photoluminescence spectra of zinc oxide, *Solid State Commun.* 128 (2003) 35–39. doi:10.1016/S0038-1098(03)00616-1.

- [20] S. Tsoi, X. Lu, A.K. Ramdas, H. Alawadhi, M. Grimsditch, M. Cardona, et al., Isotopic-mass dependence of the A, B, and C excitonic band gaps in ZnO at low temperatures, *Phys. Rev. B.* 74 (2006) 165203. doi:10.1103/PhysRevB.74.165203.
- [21] C. Gray, J. Cullen, C. Byrne, G. Hughes, I. Buyanova, W. Chen, et al., Growth of isotopically enriched ZnO nanorods of excellent optical quality, *J. Cryst. Growth.* 429 (2015) 6–12. doi:10.1016/j.jcrysgro.2015.07.003.
- [22] M. Biswas, E. McGlynn, M.O. Henry, M. McCann, a. Rafferty, Carbothermal reduction vapor phase transport growth of ZnO nanostructures: Effects of various carbon sources, *J. Appl. Phys.* 105 (2009) 94306. doi:10.1063/1.3121213.
- [23] J. Grabowska, K.K. Nanda, E. McGlynn, J.-P. Mosnier, M.O. Henry, Studying the growth conditions, the alignment and structure of ZnO nanorods, *Surf. Coatings Technol.* 200 (2005) 1093–1096. doi:10.1016/j.surfcoat.2005.01.030.
- [24] K. Govender, D.S. Boyle, P.B. Kenway, P. O'Brien, Understanding the factors that govern the deposition and morphology of thin films of ZnO from aqueous solution, *J. Mater. Chem.* 14 (2004) 2575. doi:10.1039/b404784b.
- [25] R.B. Peterson, C.L. Fields, B.A. Gregg, Epitaxial Chemical Deposition of ZnO Nanocolumns from NaOH Solutions, *Langmuir.* 20 (2004) 5114–5118. doi:10.1021/la049683c.
- [26] D. Byrne, The growth and characterisation of ordered arrays of zinc oxide nanostructures and optical studies of defects in zinc oxide, Ph.D. thesis, Dublin City University, 2012. (<http://doras.dcu.ie/16919/>).
- [27] Y.-J. Lee, T.L. Sounart, D.A. Scrymgeour, J.A. Voigt, J.W.P. Hsu, Control of ZnO

- nanorod array alignment synthesized via seeded solution growth, *J. Cryst. Growth*. 304 (2007) 80–85. doi:10.1016/j.jcrysgro.2007.02.011.
- [28] R.B. Saunders, E. McGlynn, M.O. Henry, Theoretical Analysis of Nucleation and Growth of ZnO Nanostructures in Vapor Phase Transport Growth, *Cryst. Growth Des.* 11 (2011) 4581–4587.
- [29] R.B. Saunders, S. Garry, D. Byrne, M.O. Henry, E. McGlynn, Length versus Radius Relationship for ZnO Nanowires Grown via Vapor Phase Transport, *Cryst. Growth Des.* 12 (2012) 5972–5979. doi:10.1021/cg3009738.
- [30] R.B. Saunders, Theoretical and Experimental Studies of ZnO Nanowires Grown by Vapour Phase Transport, Ph.D. thesis, Dublin City University, 2012. (<http://doras.dcu.ie/17138/>).
- [31] C. Borchers, S. Mu, D. Stichtenoth, D. Schwen, C. Ronning, Catalyst - Nanostructure Interaction in the Growth of 1-D ZnO Nanostructures, *J. Phys. Chem. B*. 110 (2006) 1656–1660. doi:10.1021/jp054476m.
- [32] D. Hou, T. Voss, C. Ronning, A. Menzel, M. Zacharias, Deep-level emission in ZnO nanowires and bulk crystals: Excitation-intensity dependence versus crystalline quality, *J. Appl. Phys.* 115 (2014) 233516. doi:10.1063/1.4884611.
- [33] D. Byrne, R. Fath Allah, T. Ben, D. Gonzalez Robledo, B. Twamley, M.O. Henry, et al., Study of Morphological and Related Properties of Aligned Zinc Oxide Nanorods Grown by Vapor Phase Transport on Chemical Bath Deposited Buffer Layers, *Cryst. Growth Des.* 11 (2011) 5378–5386. doi:10.1021/cg200977n.
- [34] M.A. Zimmler, T. Voss, C. Ronning, F. Capasso, Exciton-related electroluminescence

- from ZnO nanowire light-emitting diodes, *Appl. Phys. Lett.* 94 (2009) 241120.  
doi:10.1063/1.3157274.
- [35] E. McCarthy, R.T. Rajendra Kumar, B. Doggett, S. Chakrabarti, R.J. O’Haire, S.B. Newcomb, et al., Effects of the crystallite mosaic spread on integrated peak intensities in  $2\theta$ - $\omega$  measurements of highly crystallographically textured ZnO thin films, *J. Phys. D. Appl. Phys.* 44 (2011) 375401. doi:10.1088/0022-3727/44/37/375401.
- [36] B.-H. Hwang, Calculation and measurement of all (002) multiple diffraction peaks from a (001) silicon wafer, *J. Phys. D. Appl. Phys.* 34 (2001) 2469–2474.  
doi:10.1088/0022-3727/34/16/311.
- [37] R.T.R. Kumar, E. McGlynn, M. Biswas, R. Saunders, G. Troliard, B. Soulestin, et al., Growth of ZnO nanostructures on Au-coated Si: Influence of growth temperature on growth mechanism and morphology, *J. Appl. Phys.* 104 (2008) 84309.  
doi:10.1063/1.2996279.
- [38] JCPDS Database, Jt. Committee Powder Diffr. Stand. (n.d.). [www.icdd.com](http://www.icdd.com).
- [39] M. Hidaka, K. Ohashi, R.P. Wijesundera, L.S.R. Kumara, M. Watanabe, K. Koga, et al., Correlation between glaze-colors and structural properties of the HIZEN celadons produced in the Edo period of Japan , by means of X-ray diffraction ( I ), *Cerâmica.* 57 (2011) 106–114.
- [40] S. Desgreniers, High-density phases of ZnO: Structural and compressive parameters, *Phys. Rev. B.* 58 (1998) 14102–14105. doi:10.1103/PhysRevB.58.14102.
- [41] C.F. Klingshirn, B.K. Meyer, A. Waag, A. Hoffmann, J. Geurts, ZnO: From Fundamental Properties Towards Novel Applications, Springer-Verlag, Berlin,

- Heidelberg, 2010. doi:10.1007/978-3-642-10577-7.
- [42] H. Morkoç, U. Özgür, Zinc Oxide Fundamentals, Materials and Device Technology, Wiley-VCH, Weinheim, 2009.
- [43] J. Serrano, F. Widulle, A.H. Romero, A. Rubio, R. Lauck, M. Cardona, Dependence of phonon widths on pressure and isotopic mass : ZnO, Phys. Status Solidi. 235 (2003) 260–266. doi:10.1002/pssb.200321566.
- [44] J. Serrano, F. Manjón, A. Romero, F. Widulle, R. Lauck, M. Cardona, Dispersive Phonon Linewidths: The E<sub>2</sub> Phonons of ZnO, Phys. Rev. Lett. 90 (2003) 55510. doi:10.1103/PhysRevLett.90.055510.
- [45] S. Müller, D. Stichtenoth, M. Uhrmacher, H. Hofsäss, C. Ronning, J. Röder, Unambiguous identification of the PL-I<sub>9</sub> line in zinc oxide, Appl. Phys. Lett. 90 (2007) 12107. doi:10.1063/1.2430483.
- [46] M. Schilling, R. Helbig, G. Pensl, Bound exciton luminescence of Ar- and Al-implanted ZnO, J. Lumin. 33 (1985) 201–212. doi:10.1016/0022-2313(85)90018-3.
- [47] B.K. Meyer, H. Alves, D.M. Hofmann, W. Kriegseis, D. Forster, F. Bertram, et al., Bound exciton and donor–acceptor pair recombinations in ZnO, Phys. Status Solidi. 241 (2004) 231–260. doi:10.1002/pssb.200301962.
- [48] M. Biswas, Y.S. Jung, H.K. Kim, K. Kumar, G.J. Hughes, S. Newcomb, et al., Microscopic origins of the surface exciton photoluminescence peak in ZnO nanostructures, Phys. Rev. B. 83 (2011) 235320. doi:10.1103/PhysRevB.83.235320.
- [49] J. Cullen, D. Byrne, K. Johnston, E. McGlynn, M.O. Henry, Chemical identification of

- luminescence due to Sn and Sb in ZnO, *Appl. Phys. Lett.* 102 (2013) 192110.  
doi:10.1063/1.4807288.
- [50] B.K. Meyer, J. Sann, S. Lautenschläger, M.R. Wagner, A. Hoffmann, Ionized and neutral donor-bound excitons in ZnO, *Phys. Rev. B.* 76 (2007) 184120.  
doi:10.1103/PhysRevB.76.184120.
- [51] R. Roder, M. Wille, S. Geburt, J. Rensberg, M. Zhang, J.G. Lu, et al., Continuous wave nanowire lasing, *Nano Lett.* 13 (2013) 3602–3606. doi:10.1021/nl401355b.
- [52] U. Rössler, *Landolt-Börnstein Numerical Data and Functional Relationships in Science and Technology, Semiconductors B: II-VI and I-VII Compounds*, Springer-Verlag, Berlin and Heidelberg (on CD-ROM), 1999.
- [53] W.H. Hirschwald, Zinc oxide: an outstanding example of a binary compound semiconductor, *Acc. Chem. Res.* 18 (1985) 228–234. doi:10.1021/ar00116a001.
- [54] A.C.S. Sabioni, M.J.F. Ramos, W.B. Ferraz, Oxygen diffusion in pure and doped ZnO, *Mater. Res.* 6 (2003) 173–178. doi:10.1590/S1516-14392003000200011.
- [55] D. Byrne, F. Herklotz, M.O. Henry, E. McGlynn, Unambiguous identification of the role of a single Cu atom in the ZnO structured green band, *J. Physics. Condens. Matter.* 24 (2012) 215802. doi:10.1088/0953-8984/24/21/215802.
- [56] H. Takahashi, H. Nakamura, M. Izaki, J. Katayama, Method of forming a Cu interconnect pattern, US patent US 6607981 B1, 2003.
- [57] R.-D. Sun, A. Nakajima, A. Fujishima, T. Watanabe, K. Hashimoto, Photoinduced Surface Wettability Conversion of ZnO and TiO<sub>2</sub> Thin Films, *J. Phys. Chem. B.* 105

## HIGHLIGHTS

- High quality ZnO nanorods grown using two novel methods enriched with  $^{18}\text{O}$  isotopes
- The nanorods SEM, XRD, Raman and Photoluminescence characterization was carried out
- Morphology and crystal structure of the material is of high quality
- O-enriched ZnO is of excellent optical quality, for defect studies
- Possible explanations for the enrichment levels measured are discussed